Onset of the bound states in strange Λ, Ξ-hypernuclei and hyperspherical three-body model calculation for the corresponding double hyperon hypernuclei

M Alam[a], S H Mondal[b], M Hasan[c], Md. A Khan*[d]

[a,b,c,d] Department of Physics, Aliah University, IIA/27, Newtown, Kolkata-700160, India.

*drakhan.rsm.phy@gmail.com; drakhan.phys@aliah.ac.in

Abstract. In this work, we have explored ground state properties of ${}^{10}_{\Lambda\Lambda}$Be hypernucleus in the light of recent observation of the experiment J-PARC E07 and the onset of stability for ${}^{10}_{\Lambda\Xi}$Be hypernucleus in the three-body framework using Hyperspherical Harmonics Expansion (HHE) method. An effective core-Y (Y= Λ, Ξ) Woods-Saxon potential with adjustable depth parameter is used to reproduce the observed ground state energy of the two-body subsystem by solving the two-body Schrödinger equation. The core-Y potential so obtained is clubbed with the YY potential model of the Nijmegen group to obtain the observables of the double-hyperon hypernuclei. Computed YY separation energy and YY bond energy are compared with the data available in the literature.

1. Introduction

Hypernuclear physics is gaining popularity both in theory and in experiments, since the publication of the first discovery of Λ-hypernucleus by the Polish physicists Marion Danysz and Jerzy Pniewski [1]. Hypernuclei are subatomic systems with a remarkable strangeness degree of freedom as compared with conventional nuclei. Such exotic kinds of nuclei are formed when one or more strange exotic hyperon(s) (like Λ, Σ, Ξ, etc) are injected into an atomic nucleus to replace or more nucleon(s) of the nucleus and the injected particles are coupled to the nuclear core [2,3]. One of the remarkable effects of the hyperons is that they act as glue-like particles leading to an extension of the proton and neutron driplines and the emergence of stable exotic nuclei as discussed by Hiyama [4]. The intrusion of hyperons in unstable nuclei as an impurity give some more interesting effects in nuclear systems like the shrinkage of the nuclear size reported by Hiyama et al. [5]; deformation of nuclear shape reported by Isaka et al. [6], Lu et al. [7]; modification of cluster structure by deep penetration inside the target nucleus as reported by Hagino et al. [8]; a shift of neutron dripline towards neutron-rich side discussed by Zhou et al. [9] and occurrence of the skin or halo structure of the nucleon and hyperon Hiyama et al. [10]. Apart from those they provide useful information on hyperon-nucleon (YN) and hyperon-hyperon (YY) interactions, but precise data of YN and YY interactions are very limited due to difficulties in scattering experiments with hyperons as discussed by Vidana et al. [11], Rijken and Schulze [12], and Garcilazo [13]. Taking advantage of the significantly longer lifetimes of these strange nuclei as compared to typical reaction times, they can be helpful to investigate the models of

nuclear structure and the behavior of strange particles in the baryonic matter discussed by Sedrakian et al. [14]. The literature survey reveals that hyperons are the main constituent in the core of many stars and particularly in neutron stars when interior matter density becomes approximately double the matter density of ordinary nuclei. The YN and YY interactions have adequate demand for the solution of the equation of state (EoS) that describes the structure of a neutron star, its maximum mass, and size. Also, the interaction between hyperons takes care of additional stability conditions and cooling behavior of massive neutron stars as discussed by Schaffner-Bielich [15], Weissenborn et al. [16], and Fortin et al. [17].

Among the singly strange hypernuclei, the most extensively studied species is the single-Λ hypernuclei. So far bound states of more than 30 Λ-hypernuclei have been identified experimentally ranging from the lightest ${}^{3}_{\Lambda}\mathrm{H}$ to the heaviest ${}^{208}_{\Lambda}\mathrm{Pb}$ as reported by Juric et al. [18], Hotchi et al. [19], Gal et al. [20], and Liu et al. [21]. Danysz et al. [22] first observed the existence of double-Λ hyperfragment by the capture of a Ξ−hyperon on a light emulsion of nucleus and confirmed the low energy ΛΛ interaction. Two-Λ separation energy $S_{\Lambda\Lambda}$, ΛΛ bond energy $\Delta B_{\Lambda\Lambda}$ for the ${}^{6}_{\Lambda\Lambda}\mathrm{He}$ hypernuclei has reported by Prowse [23] and Nakazawa et al. [24] in the emulsion experiment. Ahn et al. [25] confirmed strong evidence for the production of ${}^{4}_{\Lambda\Lambda}\mathrm{H}$ in reactions on ${}^{9}\mathrm{Be}$ in experiment E906 at BNL-AGS collaboration. The production of ${}^{10-12}_{\Lambda\Lambda}\mathrm{Be}$, ${}^{13}_{\Lambda\Lambda}\mathrm{B}$ hypernuclei, their two-Λ separation ΛΛ energy $B_{\Lambda\Lambda}$ and ΛΛ bond energy $\Delta B_{\Lambda\Lambda}$ have been reported by Aoki et al. [26] with emulsion counter hybrid experiment (KEK E176), Ahn et al. [27] with nuclear emulsion and scintillating-fiber detectors (KEK-E373), Ekawa et al. [28] J-PARC E07 Collaboration and Ohnishi et al. [29] KEK-E373 (KEK-E176) experiment.

Apart from the experimental study, hypernuclear physics has also been extensively investigated theoretically. The structure of double-Λ hypernuclei such as ${}^{5}_{\Lambda\Lambda}\mathrm{H}$, ${}^{5}_{\Lambda\Lambda}\mathrm{He}$, ${}^{6}_{\Lambda\Lambda}\mathrm{He}$, ${}^{10}_{\Lambda\Lambda}\mathrm{Be}$, ${}^{13}_{\Lambda\Lambda}\mathrm{B}$ and other several hypernuclear systems adopting core + Λ + Λ three-body model in the G-matrix theory approach using various Nijmegen potential models investigated by Himeno et al. [30], Yamamoto et al. [31] and Lanskoy et al. [32]; in Hartree-Fock (HF) and variational approaches Caro et al. [33] and Nemura et al. [34]; Faddeev-Yakubovsky calculations adopting few-body cluster model Filikhin et al. [35]; five-body cluster model Hiyama et al. [5,36]. Bhowmick et al. [37] predicted the single- and double-Λ separation energies for the ground and excited states of several hypernuclei using the Relativistic Mean Field (RMF) formalism. Pal et al. [38,39] studied the binding energies in the ground and excited states of different single Λ and double-Λ hypernuclei in the light to heavy mass region within the framework of the non-relativistic Schrödinger equation. A Hulthén type of core-hyperon screening potential was used for their calculation. Also, in the last few years, microscopic calculations for these energies were carried out for light, medium and heavy nuclei in the framework of relativistic mean field (RMF). Shen et al. [40], Brueckner Hartree Fock (BHF) Schulze et al. [41], quark mean field (QMF) models Hu et al. [42], generalized mass formula Samanta et al. [43,44] and microscopic cluster model Kanada-En'yo [45], all these theoretical models provide excellent descriptions as well as good agreement with experimental data.

A hyperon-nucleus Woods-Saxon potential taken for a two-body calculation of ${}^{9}_{\Lambda}\mathrm{Be}$, we reproduced single-Λ energies B_{Λ} by adjusting the potential depth parameter which will be used to get a bound state in the three-body calculation of ${}^{10}_{\Lambda\Lambda}\mathrm{Be}$ and ${}^{10}_{\Lambda\Xi}\mathrm{Be}$ hypernucleus. One boson exchange hard core and soft-core Nijmegen potential models used for the YY interaction pair were simulated [31,32] in three-range Gaussian and two-range Yukawa forms where ΛΛ two-body systems must be unbound. The paper is organized as follows. In section 2, we introduced and discussed the HHE method for our present study of a three-body system consisting of two hyperon particles. Section 3, reported the potential used, numerical results and discussion. Finally, in section 4, we shall summarize and draw our conclusions.

2. Theoretical method

We adopted here HHE method is basically an appropriate and precise method without any approximation other than an ultimate truncation of the expansion basis due to computer memory limitations, in which any desired precision and convergence trend can be obtained by gradually increasing the size of the expansion basis [46]. The labeling scheme in this approach and choice of Jacobi coordinates for a general three-body system consisting of a relatively heavier core nucleus and two valence hyperons are shown in 'figure 1' The analytical representation of the set of Jacobi coordinates corresponding to the partition "i" in which particle labeled "i" is the spectator and those labeled as "j" and "k" form the interacting pair are:

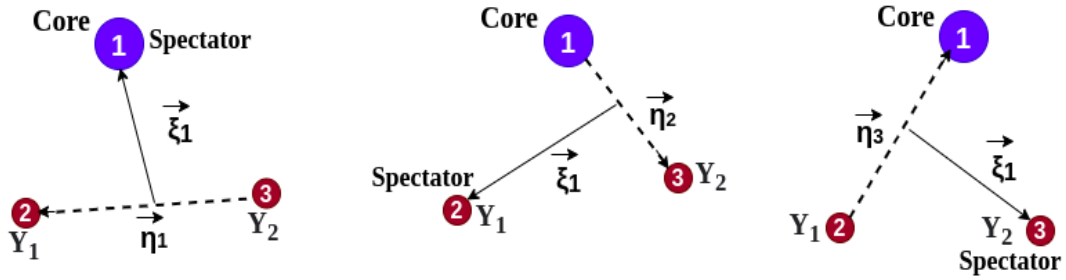

Figure 1. Label scheme and choice of Jacobi coordinates for a in general three-body configuration (CYY) in the partition "i", [i=1,2,3 - cyclic].

$$\vec{\eta_i} = \left[\frac{m_j m_k M}{m_i(m_j+m_k)^2}\right]^{\frac{1}{4}}\left(\vec{r_j} - \vec{r_k}\right) \; ; \; \vec{\xi_i} = \left[\frac{m_i(m_j+m_k)}{m_j m_k M}\right]^{\frac{1}{4}}\left(\vec{r_i} - \frac{m_j\vec{r_j} - m_k\vec{r_k}}{m_j+m_k}\right) \quad (1)$$

Where $\vec{\chi} = \sum_{i=1}^{3}\frac{m_i r_i}{M}$ is the centre of mass coordinate, M = (m_i + m_j + m_k) is the total mass of the system, and the sign of $\vec{\eta_i}$ is determined by the condition that (i, j, k) form a cyclic permutation of (1, 2, 3). Hyperspherical variables associated with the Jacobi coordinates described elaborately by Khan [46] are:

$$\eta_i = \rho\cos\Phi_i; \xi_i = \rho\sin\Phi_i$$

Where $\rho = \sqrt{{\eta_i}^2 + {\xi_i}^2}; \Phi_i = \tan^{-1}\left(\frac{\xi_i}{\eta_i}\right)$. The motion of the three-body system in relative coordinates can be described by the Schrödinger's equation

$$\left[\frac{-\hbar^2}{2\mu}\left\{\frac{\partial^2}{\rho^5} + \frac{5}{\rho}\frac{\partial}{\partial\rho} + \frac{\hat{K}^2(\Omega_i)}{\rho^2}\right\} + V(\rho,\Omega_i) - E\right]\Psi(\rho,\Omega_i) = 0 \quad (2)$$

Where $\mu = \frac{m_i m_j m_k}{M}$ is is an effective mass parameter, $V(\rho,\Omega_i) = V_{jk} + V_{ki} + V_{ij}$ is the total interaction potential, $\Omega_i = \{\Phi_i, \theta_{\eta_i}, \Phi_{\eta_i}, \theta_{\xi_i}, \Phi_{\xi_i}\}$ represents hyper-angles. The wave function $\Psi(\rho,\Omega_i)$ in any chosen partition (say in partition 'i') is expanded as

$$\Psi(\rho,\Omega_i) = \sum_{k\sigma_i}\rho^{\frac{-5}{2}}U_{k\sigma_i}(\rho)\Theta_{k\sigma_i}(\Omega_i) \quad (3)$$

where the square of hyper angular momentum operator satisfies an eigenvalue equation [76]

$$\hat{K}^2(\Omega_i)\Theta_{k\sigma_i}(\Omega_i) = K(K+4)\Theta_{k\sigma_i}(\Omega_i)$$

Where $\Theta_{k\sigma_i}(\Omega_i)$ is called the hyperspherical harmonics (HH), $n_i = \frac{\left(K - l_{\eta_i} - l_{\xi_i}\right)}{2}$, n_i being non-negative integer and the quantity K is the hyperangular momentum quantum number; $\sigma_i = \{l_{\eta_i}, l_{\xi_i}, L, M\}$ angular momenta l_{η_i}, l_{ξ_i} corresponding to η_i, ξ_i motions are coupled to give the total orbital angular momentum $\vec{L} = \vec{l_{\eta_i}} + \vec{l_{\xi_i}}$, M is the projection of $\vec{L}$. Substitution of expansion of equation (3)' in equation (2)' and use of the orthonormality of HH leads to an infinite set of couple differential equations (CDE) in ρ

$$\left[\frac{-\hbar^2}{2\mu}\frac{d^2}{d\rho^2}+\frac{\hbar^2}{2\mu}\frac{\left(K+\frac{3}{2}\right)\left(K+\frac{5}{2}\right)}{\rho^2}-E\right]U_{k\sigma_i}(\rho)+\sum_{k'\sigma_i'}M_{KK'}^{\sigma_i\sigma_i'}U_{K'\sigma_i'}(\rho)=0 \qquad (4)$$

Where $M_{KK'}^{\sigma_i\sigma_i'}=K\sigma_i|V(\rho,\Omega_i)|K'\sigma_i'\geq\int\Theta_{K\sigma_i}^{*}(\Omega_i)\,V(\rho,\Omega_i)\Omega_{K'\sigma_i'}(\Omega_i)d\Omega_i$ (5)
represents the coupling potential matrix elements. Expansion in equation (3)' is truncated to a finite set due to practical limitations, resulting in a finite set of CDE. The imposition of symmetry and conservation requirements father reduces the expansion basis to a solvable set of CDE. After the evaluation of coupling potential matrix elements following the prescription of Khan [46], the set of CDE equation (5)' is solved numerically subject to proper boundary conditions to get the energy E and the partial waves $W_{K\sigma_i}(\rho)$.

2.1. The application to $^{10}_{YY}Be$ system

In the physics of hypernuclei "critical stability" is one of the most fascinating subjects. When nucleons are added to an ordinary nucleus, they tend to be localized outside the core due to the Pauli exclusion principle whereas the core of the hypernucleus has only nucleons and when a hyperon is added to the core nucleus, no Pauli symmetry requirements under exchange of valance hyperon(s) and nucleons occur. As a result, hyperons can reach deep inside, and attract the surrounding nucleons towards the interior of the core nucleus. This "glue-like" role produces a shrinkage effect and plays a crucial role in the binding mechanism. However, symmetry requirement arises due to (a) antisymmetrization of the nuclear wave function under the exchange nucleons, which is suppressed in the choice of the core as a building block and (b) antisymmetrization of the three-body wave function under the exchange of the valence hyperons have been correctly incorporated by restricting l_{η_i} values. Most of the observed double-hyperon hypernuclei have total angular momentum J = 0, and even parity in their ground state. For spin-less nuclear core (i.e., $s_c = 0$), total spin ($S = s_c + s_Y + s_Y$) of the three-body system has two allowed values either 0 or 1, since hyperons are fermions having odd-half spins. Since, J = 0, then for S = 0, L = 0; and for S = 1, L = 1. Hence, the spectroscopic notation for the ground state of double hyperon hypernuclei is $^1S_0$ and $^3P_0$ corresponding to J = 0, S = 0, L = 0 and J = 0, S = 1, L = 1 respectively. The core nucleus being spinless, S = 0 corresponds to zero total spin of the valence hyperons (i.e., $S_{YY} = 0$), hence the spin part of the three-body wave function is antisymmetric under the exchange of spins of two hyperons, leaving the spatial part of the wavefunction symmetric under exchange of their spatial coordinates. Under pair exchange operator P_{YY}, which interchanges particles 2 and 3, $\eta_i \rightarrow -\eta_i$ and ξ_i remain unchanged. Thus, P_{YY} acts like the parity operator for the pair (YY) only. If we consider two valance hyperons in spin singlet state (which is spin anti-symmetric), the space part of their wave function must be symmetric under P_{YY}. This restricts l_{η_i} to take even values only. As for the spin singlet state, total orbital angular momentum L = 0, we must have $l_{\eta_i} = l_{\xi_i}$ = even integer. Again, $n_i = \left(l_{\eta_i} - l_{\xi_i} - K\right)/2$, for n_i is a non-negative integer, K must be even and

$$l_{\eta_i} = l_{\xi_i} = 0,2,4,\ldots\ldots,\frac{K}{2}\left[\left(\frac{K}{2}-1\right)\right] \text{ for K/2 even or odd respectively.} \qquad (6)$$

For S = 1, the two valence hyperons will be in the symmetric spin triplet state $S_{YY} = 1$ while the corresponding space wavefunction must be antisymmetric under P_{YY}, allowing only l_{η_i}= odd integral values. As, the total orbital angular momentum L = 1; $\left|\left(l_{\eta_i}-1\right)\right| \leq l_{\xi_i} \leq l_{\eta_i}-1$, but parity conservation allows $l_{\xi_i} = l_{\eta_i}$ only. Thus $n_i = \left(l_{\eta_i} - l_{\xi_i} - K\right)/2$, with ni a non-negative integer, allows only even values of K, so

$$l_{\eta_i} = l_{\xi_i} = 1,3,5,\ldots\ldots,\frac{K}{2}\left[\left(\frac{K}{2}-1\right)\right] \text{ for K/2 odd or even respectively} \qquad (7)$$

In the practical calculation, the HH expansion basis given by equation (3)' is truncated to a maximum value (K_{max}) of K and $0 \leq \left(l_{\eta_i} + l_{\xi_i}\right) \leq K$ For each allowed $K \leq K_{max}$ with K = even integers, all allowed values of l_{η_i} are included. The even values of l_{η_i} correspond to L = 0, S = 0 while the odd val-

ues of l_{η_i} correspond to L =1, S = 1. This truncates equation (4)' to a set of N coupled differential equations given by

$$\left.\begin{aligned} N = \frac{1}{8}(K_{max}^2 + 6K_{max} + 8); \text{when} \frac{K_{max}}{2} \text{ is even and} \\ N = \frac{1}{8}(K_{max} + 2)^2; \text{when} \frac{K_{max}}{2} \text{ is odd.} \end{aligned}\right\} \quad (8)$$

It follows that the number of CDE's increases in quadratic form with K_{max}, hence in practice equation (4)' is truncated to a manageable size depending on the available computer facility, and the resulting set of CDE's are solved using hyperspherical adiabatic approximation (HAA) [47].

3. Choice of Core-Λ, ΛΛ and ΛΞ potentials

For the core-Λ subsystem we have chosen Woods-Saxon potential [19] with the original parameters $V_0^{\Lambda} = -30$ MeV, $R_c = r_0 A^{1/3}$ is the radius of the core nucleus; where A is mass of the core of hyper-nucleus, $r_0 = 1.1$ fm, surface diffuseness a = 0.6 fm given by

$$V_{c-\Lambda}(r) = \frac{V_0^{\Lambda}}{1+\exp[(r-R_c)/a]} \quad (9)$$

For the two-body model of ${}^{9}_{\Lambda}$Be hypernucleus an effective core-hyperon potential is obtained by adjusting the depth parameter V_0^{Λ} to reproduce the observed single-Λ separation energy (B_Λ) for the ground state keeping other parameters alike. All these parameters will be used in the case of double-Λ and ΛΞ separation energy calculation for the three-body model of ${}^{10}_{\Lambda\Lambda}$Be and ${}^{10}_{\Lambda\Xi}$Besystems respectively. For the ΛΛ pair we choose Nijmegen group one boson exchange (OBE) hard core and softcore models [48-50] for both ΛΛ and ΛΞ interaction. In the case of the first five models, we used as an input Three-range Gaussian forms (TRG) s-wave form with parameters simulated from G-matrix calculation [31,32] given as

$$V_{\Lambda\Lambda}(r) = \sum_{i=1}^{3} V_i \exp\left(\frac{r^2}{\gamma_i}\right) \quad (10)$$

The ΛΛ interaction pair is limited to a singlet s-wave channel respecting the Pauli principle. The proper significance of three-term potential equation (10)' as the first term for i=1 represent the strength of only the attraction part, second term for i=2 control the strength of the interim midrange attractive part, and finally short-range third term for i=3 provides hard-core and soft-core repulsion strength for the respective potential model, which are excellent to produce the double-Λ separation energy and ΛΛ bond energy. The last model ESC08c used as an input two-term Yukawa potential s-wave form consists of an attractive and repulsive part with parameters obtained from the solution of three-body and four-body bound state problems in terms of Faddeev equations and generalized Gaussian variational method respectively [51].

$$V_{YY}(r) = \left(-V_a \exp(-\beta_a r) + V_r \exp(-\beta_r r)\right)/r \quad (11)$$

Table 1. Parameters of the ΛΛ interaction potential for three-range Gaussian (TRG) equation (10)' and ΛΛ and ΛΞ two-range Youkawa-type format equation (11)' where all the potential entries are in MeV and range parameters are in fm.

ΛΛ interaction for three-range Gaussian (TRG) form equation (10)'								
γ_i	V_i	NHC-D	NSC97f	NSC97e	NSC89	NHC-f	NF	NS
1.5	V_1	-5.659	-5.380	-5.227	-2.447	-1.768	-4.769	-3.622
0.9	V_2	-177.8	-157.3	-168.7	-98.60	-105.9	-91.72	-45.81
0.5	V_3	925.0	810.0	867.0	436.0	462.0	675.7	136.0
YY interaction for two-range Yukawa-type potential [ESC08c] equation (11)'								
		ΛΛ	$\beta_a = 1.74$	$V_a = 121.0$	$\beta_r = 6.04$	$V_r = 926.0$		
		ΛΞ	$\beta_a = 2.20$	$V_a = 370.0$	$\beta_r = 3.90$	$V_r = 970.0$		

3.1. Results and discussions

The effective core-Λ potential and energy parameters of the ${}^{9}_{\Lambda}$Be hypernuclei in the ground state is listed in table 2. 'Figure 2' represents the variation of (a) effective core-Λ potential for ${}^{9}_{\Lambda}$Be and (b-d) hyperon-hyperon interaction potential of various potential models with the radial distance. Also, 'figure 3' shows the three-body effective potential varies with the hyper radial distance corresponding to the Nijmegen ΛΛ potential models (a-h) for ${}^{10}_{\Lambda\Lambda}$Be and (i) for ${}^{10}_{\Lambda\Xi}$Be hypernuclei. Calculated double-Y separation energies and ΛΛ bond energies for the corresponding double-hyperon hypernucleus forming a three-body system is also presented in table 3. The incremental binding energy $\Delta B_{\Lambda\Lambda}$ and relative convergence trend β of the energy with increasing K_{max} are defined as

$$\left.\begin{aligned} \Delta B_{\Lambda\Lambda} &= B_{\Lambda\Lambda}\left({}^{10}_{\Lambda\Lambda}\mathrm{Be}\right) - 2B_{\Lambda}\left({}^{9}_{\Lambda}\mathrm{Be}\right) \\ \beta &= \frac{B(K+4) - B(K)}{B(K+4)} \end{aligned}\right\} \quad (12)$$

Table 2. Parameters of potential component generated for the core-Λ bound states using Woods-Saxon potential and corresponding single-Λ separation energy (B_Λ) for ${}^{9}_{\Lambda}$Be hypernucleus. All the parameters are in MeV unit.

	Our results			Expt.(B_Λ)	Theoretical (B_Λ)
	B_Λ	$V_0{}^{\Lambda}$	$V_{(c\text{-}\Lambda)min}$		
${}_{\Lambda}{}^{9}$Be	6.7108	-27.9963	-27.1757	6.71 ± 0.04 [18]	5.7810 [53]
				6.30 ± 0.10 [52]	$7.438^{+0.183}_{-0.223}$ [38]

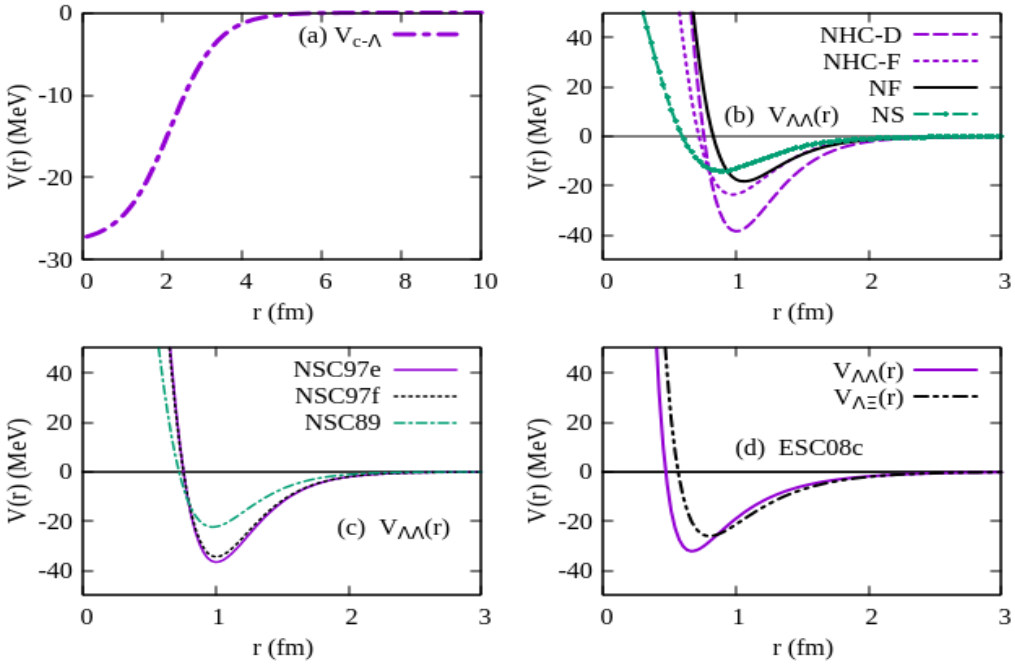

Figure 2. Plot of (a) effective core-Λ potential due to Woods-Saxon potential for ${}^{9}_{\Lambda}$Be, (b-d) ΛΛ and ΛΞ potentials for hard core and softcore Nijmegen potential models.

Table 3. Comparison of double-Λ separation energy ($B_{\Lambda\Lambda}$), ΛΛ bond energy ($\Delta B_{\Lambda\Lambda}$) with experimental results for $^{10}_{\Lambda\Lambda}$Be hypernucleus using various ΛΛ interactions models and $B_{\Lambda\Xi}$ for the predicted $^{10}_{\Lambda\Xi}$Be hypernucleus.

	Energy (MeV)	Our results for ΛΛ and ΛΞ potential models								Expt.
		NHC-D	NSC97e	NSC97f	NSC89	NHC-F	ESC08c	NF	NS	
$_{\Lambda\Lambda}{}^{10}$Be	$B_{\Lambda\Lambda}$	15.877	15.717	15.565	14.820	14.867	15.438	13.078	14.064	15.05 ± 0.09 [28]
	$\Delta B_{\Lambda\Lambda}$	2.455	2.295	2.144	1.398	1.446	2.016	-0.343	0.642	1.63 ± 0.09 [28]
$_{\Lambda\Xi}{}^{10}$Be	$B_{\Lambda\Xi}$	17.826								

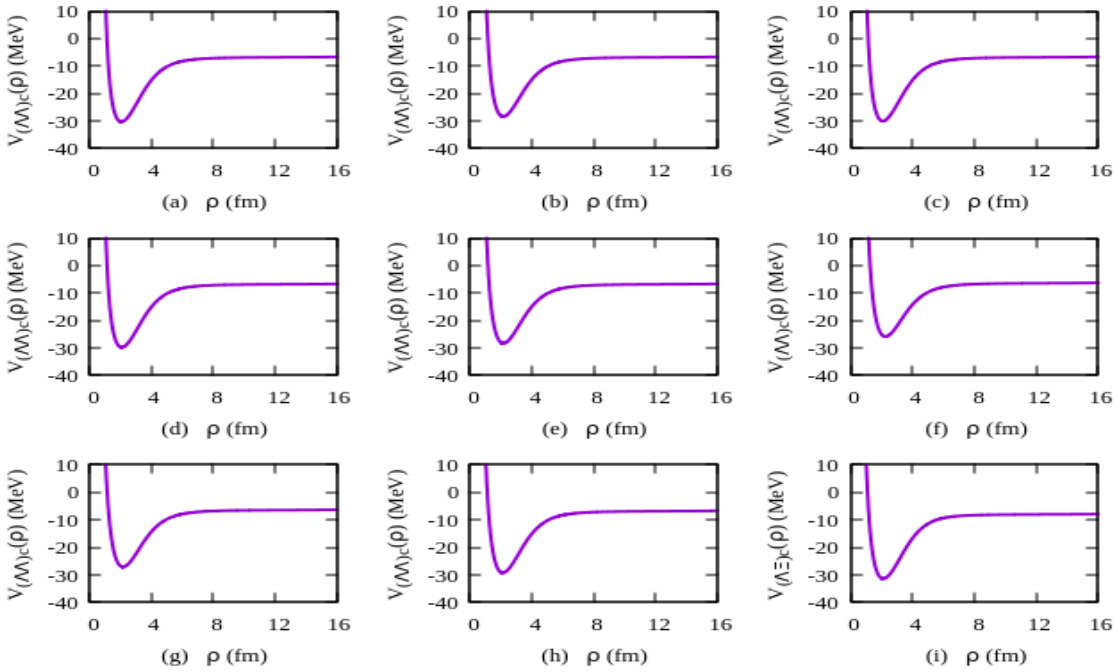

Figure 3. Three-body effective potential $V_{(\Lambda\Lambda)c}(\rho)$ as function of hyperradial distance ρ corresponding to all ΛΛ Nijmegen potential models (a) NHC-D, (b) NHC-F, (c) NSC97e, (d) NSC97f, (e) NSC89, (f) NF, (g) NS, (h) ESC08c for $^{10}_{\Lambda\Lambda}$Be and ΛΞ Nijmegen potential model (i) ESC08c for $^{10}_{\Lambda\Xi}$Be hypernucleus.

In addition to energy, some geometrical observables of the three-body system $^{10}_{\Lambda\Lambda}$Be have also been computed and listed in table 4, using the ground state wave function. These include the root mean squared (R. M. S.) radius of the three-body system defined as

$$R_{3b} = \left[\frac{A_c R_c^2 + m_\Lambda R_{c\Lambda}^2}{A_c + 2x}\right]^{1/2}$$

where A_c, m_Λ are the masses of the core and the hyperon in units of the nucleon mass, $x = m_Y$. The R. M. S. core-Λ separation is obtained using the expression $R_{c\Lambda} = \left[\left\langle r_{13}^2 + r_{12}^2 \right\rangle/2\right]^{1/2}$. The calculated energy, R. M. S. radii and correlation coefficient defined as $\vartheta = \left\langle \frac{r_{(\Lambda\Lambda)c}^2}{\rho^2} \right\rangle$ computed using the ground state wavefunction for increasing K_{max} = 0, 4, 8, ... etc. up to 24 for $^{10}_{\Lambda\Lambda}$Be are presented in table 5. A

small value of this coefficient indicates that that the two valence hyperons are positioned on two opposite sides of the core nuclei (i.e., a cigar shape where the hyperons are anti-correlated) and a relatively larger value (≤ 1) will suggest the possibility of YY correlation.

Table 4. Geometrical size parameters for K_{max} = 24 of light neutron-rich $^{10}_{\Lambda\Lambda}$Be hypernucleus for the different ΛΛ potential models.

Potential models	R.M.S. radii (fm)						ϑ
	R_{3B}	$R_{c\Lambda}$	$R_{\Lambda\Lambda}$	$R_{(\Lambda\Lambda)c}$	R_c^{CM}	R_Λ^{CM}	
NHC-D	2.2239	2.3025	3.0742	1.7143	0.3929	2.0270	0.2835
NSC97e	2.2263	2.3125	3.0946	1.7186	0.3939	2.0369	0.2825
NSC97f	2.2289	2.3235	3.1165	1.7234	0.3934	2.0476	0.2813
NSC89	2.2411	2.3743	3.2193	1.7453	0.4000	2.0978	0.2768
NHC-F	2.2400	2.3698	3.2108	1.7431	0.3995	2.0935	0.2772
ESC08c	2.2283	2.3210	3.1242	1.7166	0.3934	2.0472	0.2815
NF	2.2752	2.5116	3.4532	1.8240	0.4180	2.2266	0.2668
NS	2.2460	2.3944	3.2413	1.7625	0.4040	2.1148	0.2792

Table 5. Pattern of convergence of ΛΛ separation energy ($B_{\Lambda\Lambda}$ in MeV), relative convergence rate of energy β in equation (12), R.M.S radii and geometrical size parameters as a function of K= K_{max} = 24 of light neutron-rich $^{10}_{\Lambda\Lambda}$Be hypernucleus for the ESC08c potential models.

K_{max}	$B_{\Lambda\Lambda}$	β	R.M.S. radii (fm)						ϑ
			R_{3B}	$R_{c\Lambda}$	$R_{\Lambda\Lambda}$	$R_{(\Lambda\Lambda)c}$	R_c^{CM}	R_Λ^{CM}	
0	14.1578	0.0384	2.2297	2.3267	3.0702	1.7485	0.4007	2.0428	0.2848
4	14.7239	0.0192	2.2388	2.3648	3.1846	1.7484	0.4007	2.0861	0.2766
8	15.0118	0.0127	2.2352	2.3499	3.1659	1.7367	0.3980	2.0731	0.2785
12	15.2046	0.0078	2.2317	2.3353	3.1375	1.7299	0.3965	2.0589	0.2808
16	15.3236	0.0046	2.2298	2.3274	3.1186	1.7278	0.3960	2.0506	0.2825
20	15.3944	0.0027	2.2289	2.3237	3.1073	1.7279	0.3960	2.0464	0.2837
24	15.4365		2.2286	2.3221	3.1007	1.7288	0.3962	2.0443	0.2845

The surface and contour plot in ‘figure 4’ displays the density distribution of position probability of the hyperons and nucleons of $^{10}_{\Lambda\Lambda}$Be and $^{10}_{\Lambda\Xi}$Be hypernuclei respectively. First, from surface plots it is clearly seen that the peak of density distribution at the centre of $^{10}_{\Lambda\Xi}$Be hypernucleus is slightly higher than $^{10}_{\Lambda\Lambda}$Be hypernucleus. Second, in contour plots the contour lines figure out the nuclear density distributions while uniform background of the colour contour layers reflects that there will be a foot print of the valance hyperons in $^{10}_{\Lambda\Lambda}$Be and $^{10}_{\Lambda\Xi}$Be hypernuclei, both are looks like a deformed pear-like shape. The contour layers are more closed at the centre region of the contour plots indicates a relatively higher density arise around the nucleus. Thus, the plot also reflects an interesting fact that the hyperons are more concentrated in the vicinity of the nucleus in case of $^{10}_{\Lambda\Xi}$Be hypernucleus. Therefore, we conclude that the shrinkage effect arises due to impurity of Λ and Ξ hyperons which is theoretically investigated by Hiyama et al. [5].

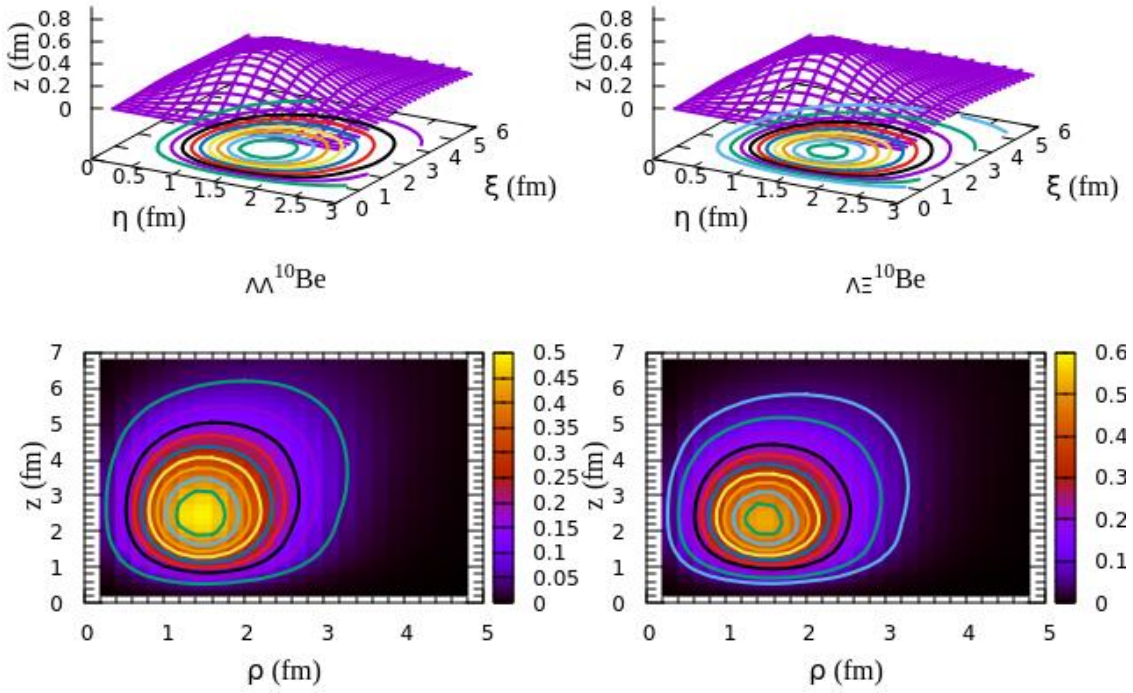

Figure 4. Surface and contour plots reflect probability density distribution of (left) Λ hyperons and nucleons for $^{10}_{\Lambda\Lambda}$Be and (right) Ξ hyperons and nucleons for $^{10}_{\Lambda\Xi}$Be with the ESC08c Nijmegen potential model.

4. Conclusion

In our present work, we estimated the ground state binding energies of $^{9}_{\Lambda}$Be, $^{10}_{\Lambda\Lambda}$Be hypernuclei and proposed a ΛΞ mixing hypernucleus $^{10}_{\Lambda\Xi}$Be. We have chosen Woods-Saxon Λ-nucleus potential for the two-body subsystem and Nijmegen model potentials for the interaction between hyperons pair in case of three-body model calculation of double hyperon hypernuclei. The results are found to be in good agreement with the experimental values (see table 2 and table 3). The estimated binding energies of $^{10}_{\Lambda\Xi}$Be corresponding to NHC-D, NSC97e, NSC97f, and ESC08c potential models are found to be slightly higher (2.578% to 5.495%) than the experimental values whereas the binding energies corresponding to NSC89, NHC-F, NF, and NS potential models are found to be slightly lower (1.216% to 13.103%) compared to the experimental findings. The binding energies of $^{10}_{\Lambda\Lambda}$Be differ from $^{10}_{\Lambda\Xi}$Be in our calculation is 2.388 MeV. The influence of additional Λ and Ξ hyperon(s) on the nuclear core has been investigated by comparing the density distribution profile between the neutron-rich nucleus $^{10}_{\Lambda\Lambda}$Be and $^{10}_{\Lambda\Xi}$Be hypernuclei. The shrinkage effect is clearly observed by the footprint of the contour plot background of the density distribution profile in 'figure 4'. In table 5, we have listed double-Λ binding energy and radius parameters which show a convergence trend up to K_{max} = 24. We will get more accurate $B_{\Lambda\Lambda}$ and ΛΛ-bond energies $\Delta B_{\Lambda\Lambda}$, higher configuration computer facilities are needed to obtain a successful convergence rate which will make the desire result. However, our method adopted here is a punchy one for the description of any nuclear or atomic few-body systems subject to the appropriate choice of two-body potentials and symmetry requirements.

Acknowledgments
Authors thankfully acknowledge University Grants Commission (UGC), New Delhi, Govt. of India for providing financial assistance and Aliah University, Kolkata, India, for providing computational facilities.

References

[1] Danysz M and Pniewski J *1953 Philos. Mag. Ser. 7* **44** 348
[2] Tamura H 2012 *Prog. Theor. Exp. Phys.* **2012** 02B012.
[3] Moradi F, Hassanabadi H, Zare S and Sobhani H 2021 *Indian J. Phys.* **95** 2431–2435
[4] Hiyama E 2003 *Few-Body Syst.* **0** 74-79
[5] Hiyama E, Kamimura M, Yamamoto Y and Motoba T 2010 *Phys. Rev. Lett.* **104** 212502
[6] Isaka M, Kimura M, Dote' A and Ohnishi A 2013 *Phys. Rev. C* **87** 021304
[7] Lu B N, Hiyama E, Sagawa H and Zhou S G 2014 *Phys. Rev. C* **89** 044307
[8] Hagino K et al. 2013 *Nucl. Phys. A* **914** 151
[9] Zhou X R, Polls A, Schulze H J and Vidaña I 2008 *Phys. Rev. C* **78** 054306
[10] Hiyama E, Kamimura M, Motoba T, Yamada T and Yamamoto Y 1996 *Phys. Rev. C* **53** 2075
[11] Vidaña I, Polls A, Ramos A and Schulze H J 2001 *Phys. Rev. C* **64** 044301
[12] Rijken Th A and Schulze H A 2016 *Eur. Phys. J. A* **52** 21
[13] Garcilazo H and Valcarce A 2016 *Phys. Rev. C* **93** 064003
[14] Sedrakian A, Weber F and Li J J *2020 Phys. Rev. D* **102** 041301(R)
[15] Schaffner-Bielich J 2008 *Nucl. Phys. A* **804** 309-21
[16] Weissenborn S, Chatterjee D and Schaffner-Bielich J 2012 *Nucl. Phys. A* **881** 62
[17] Fortin M, Avancini S S, Providência C and Vidaña I 2017 *Phys. Rev. C* **95** 065803
[18] Juric' M et al. 1973 *Nucl. Phys. B* **52** 1-30
[19] Hotchi H et al. 2001 *Phys. Rev. C* **64** 044302
[20] Gal A, Hungerford E V and Millener D J 2016 *Rev. Mod. Phys.* **88** 035004
[21] Liu P et al. 2019 *Chinese Phys. C* **43** 124001
[22] Danysz M et al. 1963 *Nucl. Phys.* **49** 121-32
[23] Prowse D J 1966 *Phys. Rev. Lett.* **17** 782
[24] Nakazawa K et al. *2010 Nucl. Phys.* A **835** 207
[25] Ahn J K et al. 2001 *Phys. Rev. Lett.* **87** 132504
[26] Aoki S et al. 2009 *Nucl. Phys. A* **828** 191-232
[27] Ahn J K et al. 2013 *Phys. Rev. C* **88** 014003
[28] Ekawa H et al. 2019 *Prog. Theor. Exp. Phys.* **2019** 021D02
[29] Ohnishi A et al. 2020 *Prog. Theor. Exp. Phys.* **2020** 063D01
[30] Himeno H, Sakuda T, Nagata S and Yamamoto Y 1993 *Prog. Theor. Phys.* **89** No.1 109
[31] Yamamoto Y et al. 1994 *Prog. Theor. Phys. Suppl.* **117** 361
[32] Lanskoy D E and Yamamoto Y 2004 *Phys. Rev. C* **69** 014303
[33] Caro J, Garcfa-Recio C and Nieves J 1999 *Nucl. Phys. A* **646** 299-342
[34] Nemura H, Suzuki Y, Fujiwara Y and Nakamoto C 2000 *Prog. Theor. Phys.* **103** No. 5 929
[35] Filikhin I N and Gal A 2002 *Nucl. Phys. A* **707** 491-509
[36] Hiyama E et al. 2010 *Prog. Theor. Phys. Suppl.* **185** 152-96
[37] Bhowmick B, Bhattacharyya A and Gangopadhyay G 2012 *Int. J. Mod. Phys. E* **21** 1250069
[38] Pal S, Ghosh R, Chakrabarti B and Bhattacharya A 2017 *Eur. Phys. J. Plus* **132** 262
[39] Pal S, Ghosh R, Chakrabarti B and Bhattacharya A 2020 *Eur. Phys. Scr.* **95** 045301
[40] Shen H, Yang F and Toki H 2006 *Prog. Theor. Phys.* **115** 325
[41] Schulze H -J and Rijken T 2013 *Phys. Rev. C* **88** 024322
[42] Hu J N, Li A, Shen H and Toki H 2014 *Prog. Theor. Exp. Phys.* **2014** 013D02
[43] Samanta C 2018 *Eur. Phys. J. Web Conf.* **182** 02107
[44] Samanta C and Schmitt T A 2019 *AIP Conf. Proc.* **2130** 040004

[45] Kanada-En'yo Y 2018 *Phys. Rev. C* **97** 034324
[46] Khan Md A 2012 *Eur. Phys. J. D* **66** 83
[47] Das T K, Coelho H T and Fabre de la Ripelle M 1982 *Phys. Rev. C* **26** 2281
[48] Maessen P M M, Rijken T A and Swart J J de 1989 *Phys. Rev. C* **40** 2226
[49] Rijken T A, Stoks V G J and Yamamoto Y 1999 *Phys. Rev. C* **59** 21
[50] Nagels M M, Rijken T A, and Swart J. J. de 1979 *Phys. Rev. D* **20** 1633
[51] Garcilazo H, Valcarce A and Vijande J 2017 *Rev. Mex. Fix.* **63** 411-422
[52] Botta E, Bressani T and Feliciello A 2017 *Nucl. Phys. A* **960** 165
[53] Santhosh K P and Nithya C 2018 *Eur. Phys. J. Plus* **133** 343